processes

MDPI

Article

Microemulsion vs. Precipitation: Which Is the Best Synthesis of Nickel–Ceria Catalysts for Ethanol Steam Reforming?

Cristina Pizzolitto [1], Federica Menegazzo [1], Elena Ghedini [1], Arturo Martínez Arias [2], Vicente Cortés Corberán [2] and Michela Signoretto [1,*]

[1] CATMAT Lab, Department of Molecular Sciences and Nanosystems, Ca' Foscari University Venice and INSTM RU of Venice, via Torino 155, Mestre, I-30172 Venezia, Italy; cristina.pizzolitto@unive.it (C.P.); fmenegaz@unive.it (F.M.); gelena@unive.it (E.G.)

[2] Institute of Catalysis and Petroleum Chemistry (ICP), CSIC, Calle Marie Curie 2, 28049 Madrid, Spain; amartinez@icp.csic.es (A.M.A.); vcortes@icp.csic.es (V.C.C.)

* Correspondence: miky@unive.it

Abstract: Ethanol steam reforming is one of the most promising ways to produce hydrogen from biomass, and the goal of this research is to investigate robust, selective and active catalysts for this reaction. In particular, this work is focused on the effect of the different ceria support preparation methods on the Ni active phase stabilization. Two synthetic approaches were evaluated: precipitation (with urea) and microemulsion. The effects of lanthanum doping were investigated too. All catalysts were characterized using N_2-physisorption, temperature programmed reduction (TPR), XRD and SEM, to understand the influence of the synthetic approach on the morphological and structural features and their relationship with catalytic properties. Two synthesis methods gave strongly different features. Catalysts prepared by precipitation showed higher reducibility (which involves higher oxygen mobility) and a more homogeneous Ni particle size distribution. Catalytic tests (at 500 °C for 5 h using severe Gas Hourly Space Velocity conditions) revealed also different behaviors. Though the initial conversion (near complete) and H_2 yield (60%, i.e., 3.6 mol H_2/mol ethanol) were the same, the catalyst prepared by microemulsion was deactivated much faster. Similar trends were found for La-promoted supports. Catalyst deactivation was mainly related to coke deposition as was shown by SEM of the used samples. Higher reducibility of the catalysts prepared by the precipitation method led to a decrease in coke deposition rate by facilitating the removal of coke precursors, which made them the more stable catalysts of the reaction.

Keywords: ethanol steam reforming; Ni/CeO_2; microemulsion; coke resistance; lanthanum doping

Citation: Pizzolitto, C.; Menegazzo, F.; Ghedini, E.; Martínez Arias, A.; Cortes Corberan, V.; Signoretto, M. Microemulsion vs. Precipitation: Which is the Best Synthesis of Nickel-ceria Catalysts for Ethanol Steam Reforming? *Processes* **2021**, *9*, 77. https://doi.org/10.3390/pr9010077

Received: 13 November 2020
Accepted: 26 December 2020
Published: 31 December 2020

1. Introduction

Hydrogen, one of the most useful intermediate products, can be the ideal candidate to solve the environmental problems [1]. Although, it is not a fuel by itself, it is considered as the future energy vector owing to its great potential for generating electricity by fuel cells [2]. A critical issue in the use of hydrogen for energy applications is its production method. In fact, despite hydrogen being the most abundant element in the universe, it does not exist in significant amounts in its elemental form [3,4]. Therefore, it must be produced from other sources. Nowadays, 96% of the hydrogen produced worldwide derives from the conversion of fossil resources [5], mainly from natural gas by steam reforming. Nevertheless, one potential for the future is the possibility of hydrogen generation from renewable sources. Among the most attractive processes, the steam reforming of light alcohols such as methanol and ethanol plays a key role [6]. Indeed, methanol can be produced by syngas derived from biomass, while ethanol can be generated by fermentation of carbohydrate sources [7]. In addition to the said use of

renewable raw materials, the use of alcohol as the main resource for hydrogen production has many advantages such as low cost, easy transportation in liquid form and the possibility of its conversion to hydrogen in relatively mild reaction conditions [8] with highly efficient and cost-effective processes. For example, conversion of ethanol into hydrogen via steam reforming provides six moles of hydrogen per mole of ethanol because it can extract hydrogen not only from ethanol but also from water ($CH_3CH_2OH + 3H_2O = 2CO_2 + 6H_2$) [9–11]. However, ethanol steam reforming (ESR) follows a complex reaction pathway, summarized in Figure 1. As may be seen, several by-products such as carbon monoxide, methane, ethylene, acetaldehyde and more complex carbon species can be generated under reaction conditions [12]. For this reason, the catalyst formulation is not a trivial task: it should be properly formulated to be functional to direct the reaction to maximize hydrogen yield and, at the same time, to suppress the unwanted side reactions. Common catalysts for ESR are metals, such as Pt, Pd, Rh, Ni, Co and Cu, [13,14] supported on different oxides, mainly Al_2O_3, SiO_2, CeO_2, ZrO_2, TiO_2, MgO and La_2O_3 [15–17] ¹¹¹⁴¹². Among them, nickel is an attractive active phase for its low cost and high activity, comparable to that of noble metals. In addition, ceria is an interesting support since it belongs to the partially reducible oxides (PROs) [8]. Indeed, it is commonly used in different oxidation reactions such as CO oxidation [18], preferential oxidation (PROX) of CO for hydrogen purification [19], water gas shift (WGS) reaction, as well as oxygen-conducting membranes for solid oxide fuel cells and many other processes [20,21]. Thanks to the redox ability and strong interaction with nickel, ceria has been extensively studied in the reforming field [22]. Ceria redox ability can be modulated by a careful control of structural defects [23–25]: the higher the number of defective sites, the more effective the redox pump. Therefore, lanthanum oxide has been added as promoter due to its possible substitution as La^{3+} in the Ce^{4+} lattice [18] which may lead to the formation of defective sites.

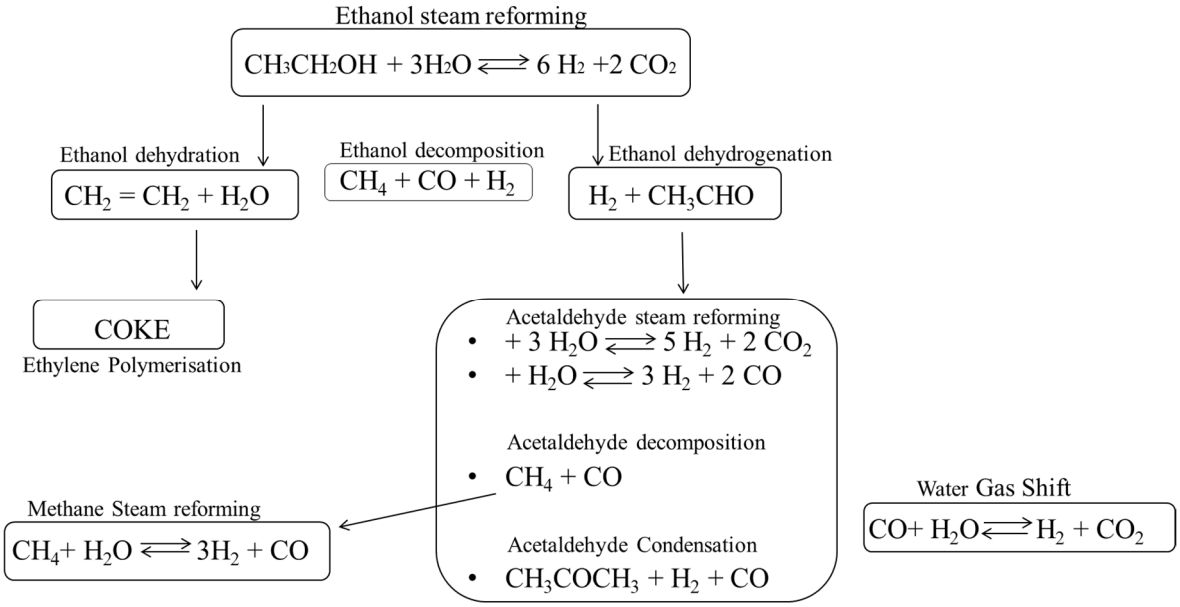

Figure 1. Reaction pathways involved in the ethanol steam reforming (ESR) process.

This work has been focused on the preparation method of the support for nickel–ceria-based catalysts. Two different synthetic methods have been investigated for ceria supports preparation: precipitation and reverse microemulsion. Precipitation is the standard approach used for metal oxides preparation. With this method, however, it is difficult to control particle size distribution. On the contrary, reverse microemulsion can be an innovative way to modulate and control the textural properties of new materials.

This approach is based on the formation of nanospherical micelles inside which the precipitation of the oxide takes place. In this way, as reported by Eriksson et al. [26], a suitable environment for producing small nanoparticles with narrow size distribution can be generated. Accordingly, the motivation of this work is to focus on the investigation of the influence of the preparation method on the activity, stability and regenerability of nickel–ceria-based catalysts for hydrogen production via ESR, that was investigated under severe Gas Hourly Space Velocity (GHSV) conditions. To the best of our knowledge this is the first use in ESR of Ni supported on La doped CeO_2 prepared by reverse microemulsion. To achieve this goal, different characterization approaches were used. In particular, the correlation between the synthetic method and structural and morphological properties was investigated by N_2-physisorption, SEM, XRD, and H_2-temperature programmed reduction (TPR). The effects of lanthanum doping have been investigated too.

2. Experimental Part

2.1. Support Preparation

Precipitation method*:* the supports (hereinafter denoted as Ce P and CeLa P) were synthesized by precipitation with urea at 100 °C with aqueous solutions of $(NH_4)_2Ce(NO_3)_6$ (Sigma Aldrich, St Louis, MO, USA) and additionally $La(NO_3)_3.6H_2O$, in the adequate amount to obtain a 5 wt % of lanthanum(Sigma Aldrich, St Louis, MO, USA); in the final sample, for the latter. The solution was mixed and boiled at 100 °C for 6 h. The precipitates were washed with deionized water and dried at 110 °C for 18 h. The material was then calcined under air flow (30 mL/min) at 650 °C for 3 h.

Reverse microemulsion method*:* the supports (hereinafter denoted as Ce M and CeLa M) were synthesized by preparing two different microemulsion systems: (A) Saline microemulsion composed by: 450 mL n-heptane 99% (Sigma Aldrich, GMBH, Riedstr, Germany), 90 mL triton X(Sigma Aldrich, St Louis, USA, MO, USA), 92 mL 1-hexanol 98% (Sigma Aldrich, St Louis, MO, USA), 50 mL aqueous solution of $Ce(NO_3)_3.6H_2O$ (0.5 M); (B) Basic microemulsion composed by 450 mL n-heptane 99%, 1-hexanol 98%, 90 mL Triton X-100 and 50 mL basic solution (0.5 M NaOH). The proper amount of lanthanum precursor was added to obtain a 5 wt % of lanthanum in the final sample. Both microemulsions were stirred at 100 rpm for 1 h. Then, solution B was added to solution A and was kept under stirring at 100 rpm for 24 h. The precipitates were separated by centrifugation, washed with methanol, dried at 120 °C for 18 h and calcined in air at 650 °C for 3 h.

2.2. Catalyst Preparation

Nickel was introduced on the supports by incipient wetness impregnation with a proper amount of $Ni(NO_3)_2.6H_2O$ aqueous solution to obtain 8 wt % of nickel on the catalysts. After drying at 110 °C for 18 h, calcination was performed in air at 650 °C for 4 h.

2.3. Catalysts Characterization

Specific surface areas and pore size distributions were evaluated by N_2 adsorption/desorption isotherms at −196 °C using a Tristal II Plus Micromeritics. (Micromeritics, Milan, Italy); The surface area was calculated using the Brunauer–Emmett–Teller (BET) Equation [27] method while pore size distribution was determined by the BJH (Barrett, Joyner, and Halenda) method [28], applied to the N_2 desorption branch of the isotherm.

The Ni and La contents were determined by atomic absorption spectroscopy (AAS) after microwave disaggregation of the samples (100 mg), using a Perkin-Elmer Analyst (Perkin-Elmer, Waltham, MA, USA); 100 spectrometer.

The morphology of the catalysts was studied by scanning electron microscopy (SEM) with a table-top Hitachi instrument, model TM-1000 (Hitachi, Ramsey, NJ, USA), after depositing the ground powder sample on a double-sided lacey carbon ribbon.

X-ray diffractograms were obtained on a Seifert XRD 3000P diffractometer; using nickel-filtered Cu Kα radiation operating at 40 kV and 40 mA, using a 0.02° step size and 2 s counting time per step. Analysis of the diffraction peaks was conducted with the software ANALYZE Rayflex Version 2.293.

Temperature programmed reduction (TPR) measurements were carried out using lab-made equipment: samples (100 mg) were heated with a temperature rate of 10 °C/min from 25 °C to 900 °C in a 5% H_2/He flow (40 mL/min). The effluent gases were analyzed by a Thermal Conductivity Detector (GOW-MAC InstrumentCo., Shannon, Irland)

2.4. Catalytic Tests

Catalysts were tested for ESR at 500 °C and atmospheric pressure, charging the feed with molar composition of water:ethanol:He = 18.4:3.1:78.5 and W/F = 0.12 $g_{cat.}$h/mol ethanol, in a stainless steel, fixed bed tubular reactor placed in an equipment Microactivity Reference model MAXXXM3-(PID Eng and Tech, Madrid, Spain). Prior to the reaction, fresh catalyst samples were activated under flow of 10% O_2 in He at 650 °C for 1 h. Catalytic stability tests were conducted at 500 °C for 5 h. After the first run, the catalyst was cooled down and flushed under inert flow, and then reactivated using the same procedure of the initial activation, heating up to 650 °C at 10 °C/min and keeping this temperature for 1 h, under a flow of 10% O_2 in He. After cooling down to 500 °C in inert flow, a second run was conducted with the regenerated samples under the same condition of the first run. Tests for each sample were reproducible within experimental error. Reactants and products were analyzed online by GC on a Varian Star 3400 CX instrument (Varian, Cridersville, OH, USA); equipped with two columns, molecular sieve and Porapak Q and the detector of thermal conductivity. After the analysis, conversion of ethanol and hydrogen yield were calculated as follows:

Conversion of ethanol:

$$conversion\ (\%) = [\frac{n_{in}(EtOH) - n_{out}(EtOH)}{n_{in}(EtOH)}] \times 100 \quad (1)$$

H_2 yield:

$$yield\ (\%) = \frac{fH2\ out}{6 \times fEtOHin} \times 100 \quad (2)$$

with n number of moles; f, flux in mL/min.

3. Results and Discussion

3.1. Catalysts Characterization

The specific surface area is one of the most important parameters in the design of a heterogeneous catalyst: a high surface area greatly improves the dispersion of the active phase [29,30]. Figure 2 shows N_2-physisorption isotherms of the samples, while the calculated values of specific surface area, mean pore radius and pore volume are reported in Table 1.

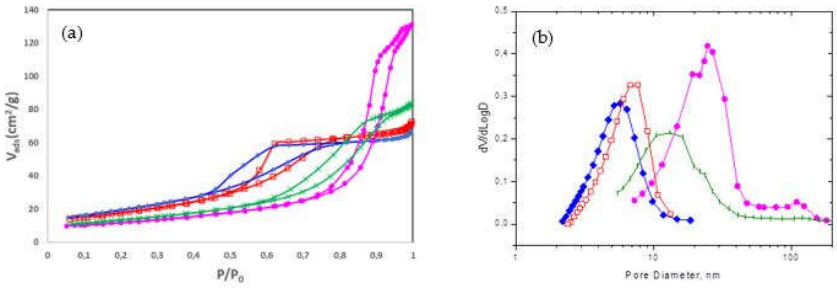

Figure 2. N_2-physisorption isotherms of catalysts (**a**) and their pore size distributions (**b**): NiCe P (red squares); NiCe M (green cross); NiLaCe P (blue rhombs); NiLaCe M (violet circle).

Table 1. Physico-chemical properties of the catalysts.

Samples	S_{BET} [a] (cm^3/g)	Mean Pore Diameter [b] (nm)	V_{pore} [c] (cm^3/g)	NiO Mean Particle Size [d] (nm)
NiCe P	64	7.0	0.11	27
NiLaCe P	71	6.8	0.12	25
NiCe M	48	10.5	0.12	15
NiLaCe M	42	12.0	0.16	14

(a) Specific surface area calculated via BET; (b) average pore diameter, and (c) pore volume calculated via BJH method; (d) calculated by Scherrer Equation.

All samples exhibited the IV-type isotherm that is typical of mesoporous materials according to IUPAC classification [31]. However, the shapes and hysteresis loops of the isotherms were quite different. The hysteresis loop of precipitated samples is H2 type, characteristic of solids with pores of irregular shape and dimension. Conversely, the catalysts obtained by the microemulsion approach show a hysteresis profile more difficult to classify being a combination of H2 and H3 hysteresis loops associated with a complex pores structure. H3 loops are, generally, associated with non-rigid aggregates of plate-like particles (e.g., certain clays) or with a pore network consisting of macropores that are not completely filled with pore condensate [32]. The pore size distribution obtained by BJH is consistent with the N_2 adsorption-desorption profiles, in fact the pore size distribution for the "M" type catalysts was broader and at higher values, at the limit of macroporosity, than for LaCe P and NiLaCe P samples. Moreover, both precipitated samples exhibit a higher BET surface area than the catalysts obtained by the microemulsion approach (Table 1).

Analytical Ni amount was the same for all the samples (7.5 wt %), only slightly lower than the nominal value of 8 wt %. As for La amount, it was around 5 wt %. The particles morphology and catalyst size were determined using microscopy techniques. Figure 3 shows SEM images of the fresh samples. As can be seen, the appearance of the materials prepared by different techniques was notably different. Samples synthesized by precipitation were made of agglomerated spherical particles of 1.8–2 μm, while catalysts prepared by microemulsion presented a wrinkled surface covered by small superficial cubic particles.

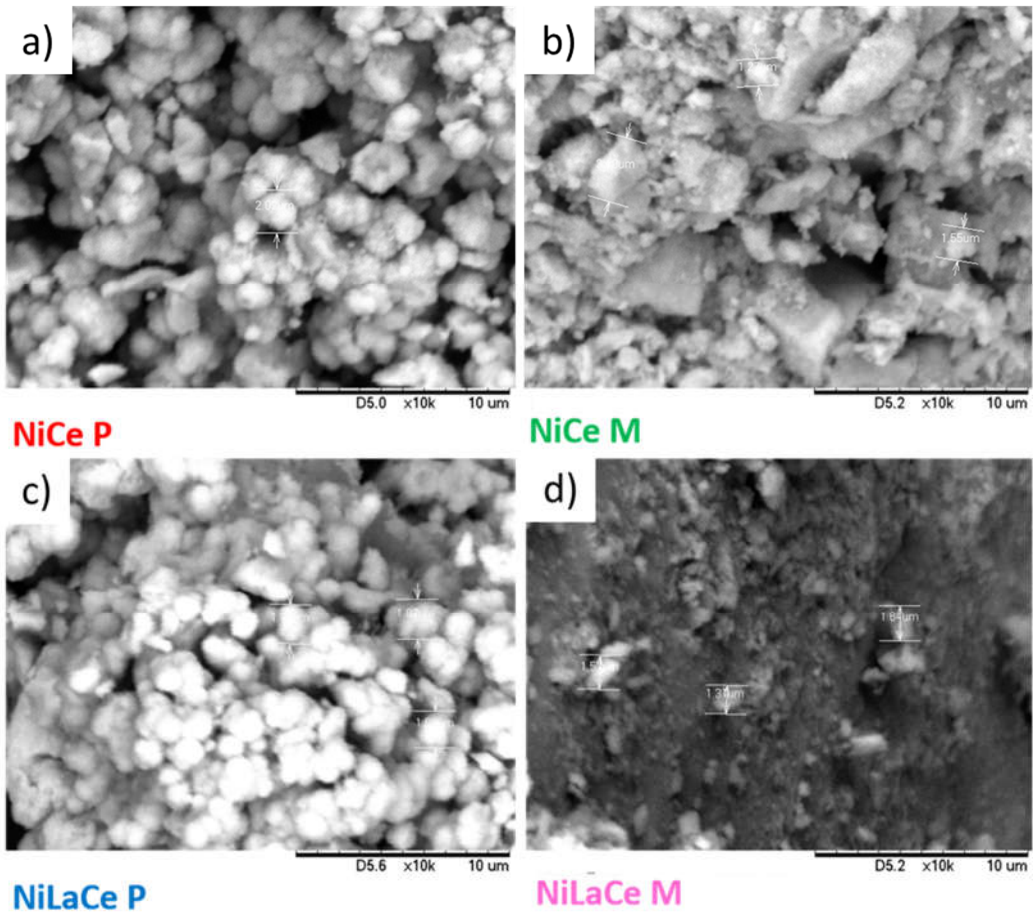

Figure 3. Representative SEM images of fresh catalysts (**a**) NiCe P, (**b**) NiCe M, (**c**) NiLaCe P and (**d**) NiLaCe M.

XRD analyses using Scherrer refinement were carried out to determine the crystal size of the support and the metal phases in the samples. Figure 4 compares the XRD patterns of the four NiCe samples prepared via different support preparation methods.

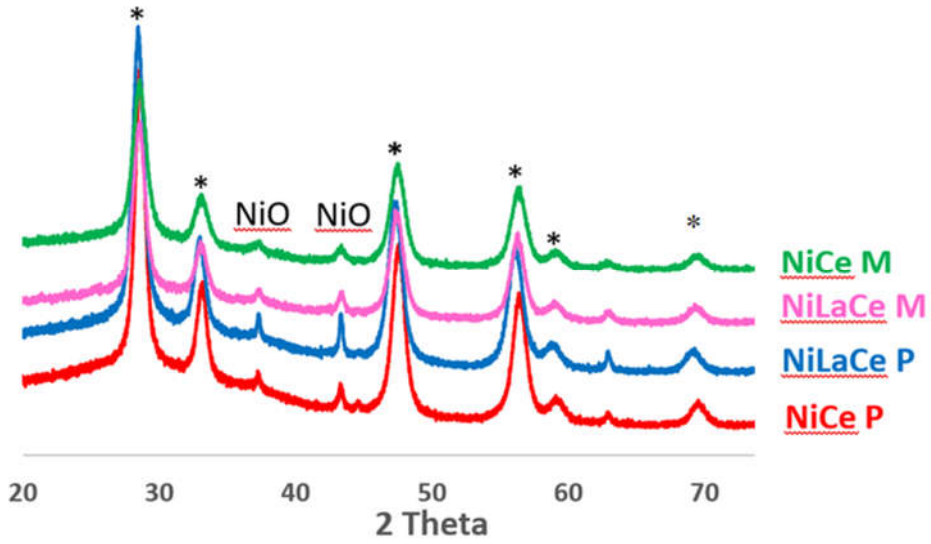

Figure 4. XRD patterns of fresh catalysts after calcination. (* denoted peaks of ceria crystal phases.)

As for the fresh samples, XRD profiles showed a fluorite-type phase of ceria with characteristic reflections at 2θ = 28°, 33°, 47°, 56°, 59°, and 69° associated with (111), (200), (220), (311), (222) and (400) planes of the cubic phase, respectively [33]. No diffraction lines related to lanthanum nor lanthanum oxide can be evidenced in XRD spectra, despite its almost 5 wt % loading. This could be reasonably due to the incorporation of La^{3+} ions in the ceria lattice [18]. A mean size of 11 and 9 nm was calculated by Sherrer for the crystal particle size of CeO_2, respectively, in NiCeP and NiCeM. La addition does not significantly affect ceria size. Regarding the active phase, the occurrence of NiO was clearly detected, with the characteristic diffraction lines at 2θ 37° and 43.4° [34]. The presence of nickel in its oxidic form was not unexpected, because the analyses have been performed on calcined catalysts, as the samples charged in the reactor for catalytic ESR testing. Table 1 shows the crystal size of NiO, calculated from the analysis of the most intense diffractions, corresponding to 2θ = 43.4°. The patterns of the precipitated samples showed sharper and more intense diffraction lines, meaning that the particles of ceria and NiO were bigger and more crystalline than for the catalysts prepared via microemulsion (Table 1).

These preliminary analyses indicated that the support preparation method strongly affected morphological and structural features of the final catalysts. Therefore, further characterizations were performed. TPR technique was used to identify the different NiO species on the ceria surface and their reduction features and to determine the support reduction temperature. The TPR profiles are reported in Figure 5. The most evident difference between the TPR profiles of the two different techniques is the number of NiO species interacting with the support. The profiles of samples prepared by precipitation presented three broad reduction peaks at 204 °C, 249 °C and 329 °C that can be associated with NiO reduction. On the contrary, the TPR curves of samples synthesized by microemulsion showed only one sharp peak centered at 470 °C. Therefore, TPR analyses clearly showed that the synthetic approach has a deep effect on Ni reducibility, which could affect their catalytic behavior. NiO was reduced at temperatures below 400 °C for samples prepared by precipitation, while for catalysts synthesized by microemulsion the temperature needed for NiO reduction is at least 400 °C. This difference can be reasonably ascribable to the different metal–support interactions that can be formed during the oxide precipitation: the stronger the interaction, the higher the reduction temperature. The broad maxima at higher temperatures are related to the support, since it is known that the ceria can be reduced from Ce^{4+} to Ce^{3+} at temperatures above 700 °C [35]. As reported in the literature, one can envisage, for the precipitated supports, one small and broad peak at 800 °C, while for the support synthesized by microemulsion, there are two small and broad peaks at 750 and 1000 °C, respectively.

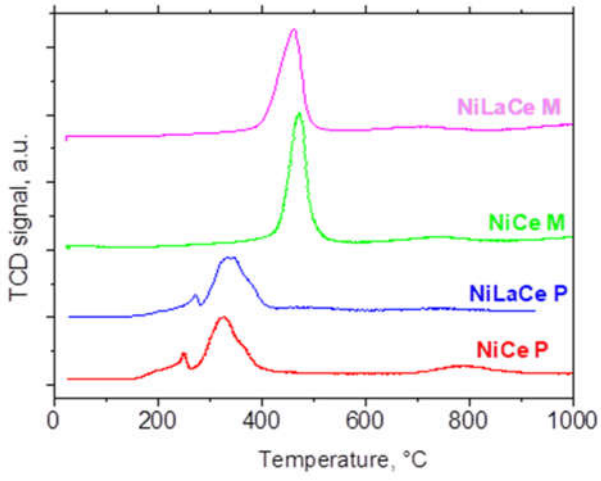

Figure 5. Temperature programmed reduction (TPR) profiles of catalysts.

From all these characterization results, remarkable differences between two methodologies have arisen. Precipitation results in slightly higher surface areas, well-defined spherical-shaped particles and high crystallinity. At the same time, catalysts prepared by this technique presented a weaker metal support interaction, and a consequent easier metal reducibility. In contrast, NiCe M and NiLaCe M showed smaller NiO dimensions and only one stronger NiO interaction with the support, which could strongly affect NiO reducibility in reaction conditions. The effect of lanthanum addition is minimal with respect the difference in the preparation methodology. Consequently, it can be affirmed that the support preparation method strongly influences morphological, structural, and chemical properties of the final catalysts.

3.2. Catalytic Performances

ESR catalytic tests were carried out at 500 °C and atmospheric pressure using severe GHSV conditions. Figure 6 reports ethanol conversion (straight line) and hydrogen yield (dotted lines) along 5 h of time on stream. Both NiCe P and NiCe M catalysts presented a high initial activity with nearly complete ethanol conversion and 60% of hydrogen yield, considering that NiCe M has a slightly lower performance than NiCe P. This could be due to a more difficult reducibility of Ni in the sample prepared by microemulsion, as was demonstrated by TPR analyses. In fact, it should be noted that these materials were not reduced before the reaction test and it is relevant to verify the reducing power of ethanol, confirming what was previously demonstrated by Pizzolitto et al. [18].

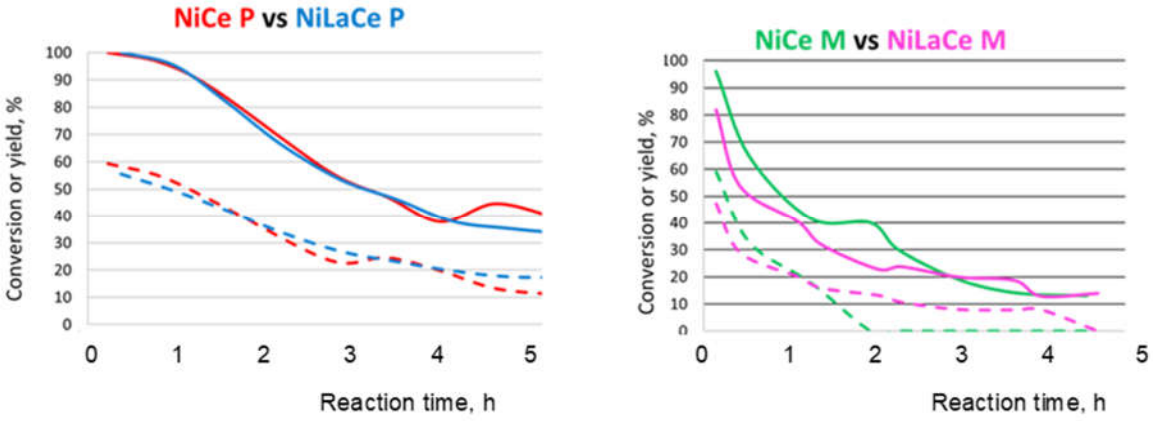

Figure 6. Catalytic activity in the ethanol steam reforming on NiLaCe P (left) and NiLaCe M (right) catalysts in comparison with the non-doped samples: ethanol conversion (full line) and hydrogen yield (dotted line).

Nevertheless, both the catalysts suffered a progressive deactivation over time on stream. However, the deactivation presented a different degree: after 2.5 h, NiCe M completely lost its activity for hydrogen production, maintaining at the same time a very low ethanol conversion. The catalyst prepared via precipitation kept 50% conversion and 30% hydrogen yield after 5 h on stream. The behavior of lanthanum-doped samples was very similar to the corresponding non-doped catalysts under the tested reaction conditions.

Characterizations of catalyst samples recovered after reaction were also performed to understand more deeply the evolution of catalytic behavior. Examples of SEM images of used samples are shown in Figure 7. As can be seen, the catalyst prepared via microemulsion, NiCe M, was almost completely covered by carbon, while the sample prepared by precipitation, NiCe P, still showed a very clear surface despite the fact that it had some dark agglomerates associated with carbon deposits. Although Carbon was not formed as nanotubes or nanowires, it was in a more compact form, either polymeric or graphitic. These results perfectly matched with the catalytic results: the complete activity loss for the NiCe M sample is due to the complete coverage of active sites by carbon. On the contrary, only a small portion of metals was covered by coke deposits, and therefore the sample was still active after 5 h of reaction.

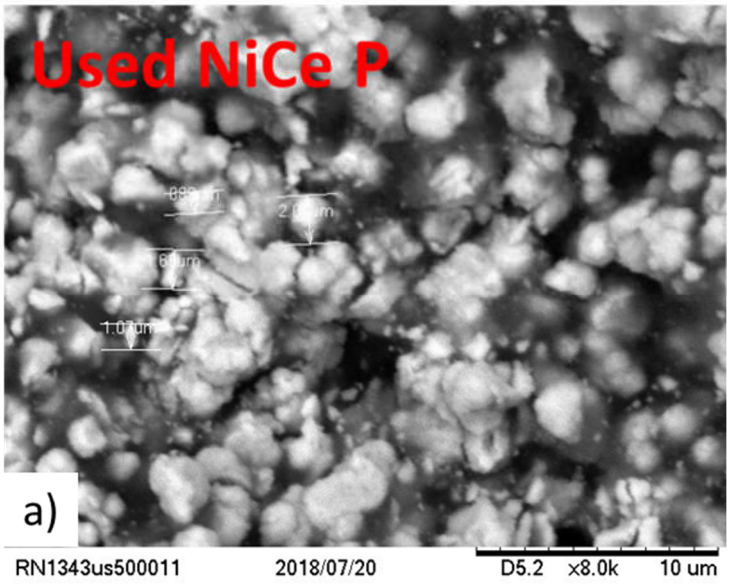

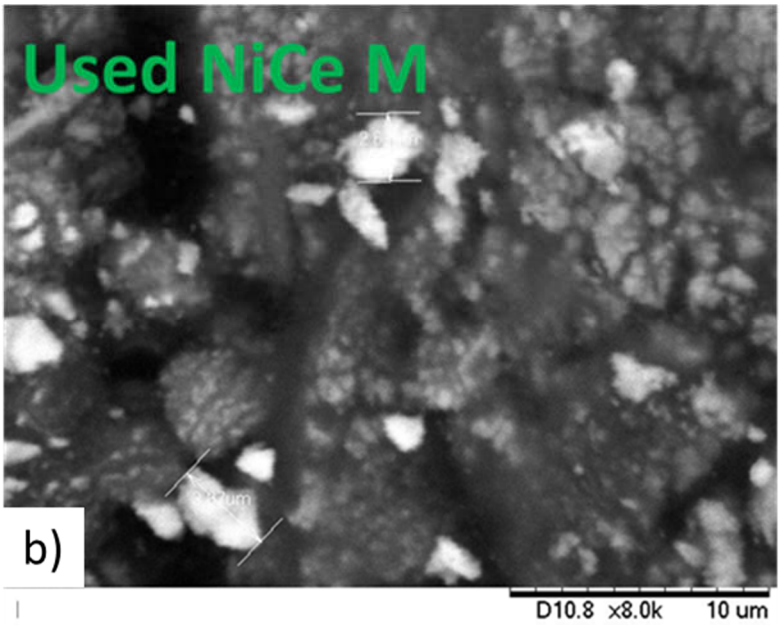

Figure 7 SEM images of used catalyst samples recovered after ethanol steam reforming tests: (**a**) Used NiCe P and (**b**) Used NiCe M.

To further understand the reasons of this discrepancy in catalytic behavior, X-ray diffractograms of the used catalysts were obtained. Figure 8 compares the XRD patterns of fresh and used catalysts from both preparation methods. The patterns of used samples presented reflections attributed to carbon species at 2θ 26.4° [36] probably with a graphite-like structure. For the used catalysts, the crystal particle size of CeO_2 slightly increased (11 and 10 nm, respectively, for used NiCe P and NiCe M) and the reflections attributed to metallic Ni appear at 2θ of 44.5° and 51.8°, while those of NiO at 43.4° disappear (see inset in Figure 8). This evidenced that the reaction mixture, that is the reactant ethanol, allowed the reduction in the metal phase, thus activating the catalysts for the reaction.

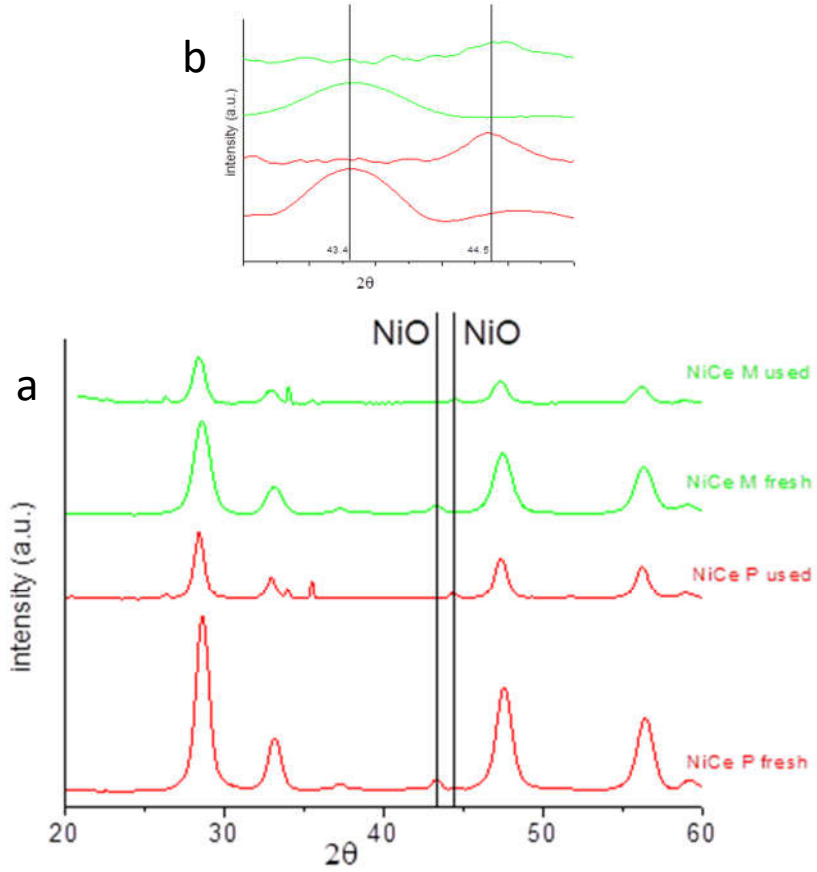

Figure 8. (**a**) XRD patterns of fresh and used catalysts after calcination. (Reflections at 2θ 35° are due to remains of SiC used as diluent in the catalytic bed.) and (**b**) magnification on reflections of NiO at 2θ 43.3 and 44.5 °.

Moreover, to determine the possibility of reusability of the catalysts, reactivation of used catalysts was carried out, followed by a second run of the catalytic test. Figure 9 compares ethanol conversion and hydrogen yield of fresh and used catalysts for both un-doped materials. After the regeneration in air, the initial H_2 yield on NiCe P, the most active one, was lower than that of the fresh sample, decreasing to 17% after 5 h of reaction (instead of 30% of the first run). Therefore, catalyst regeneration did not allow its complete reactivation, indicating either possible sintering of the catalyst or incomplete removal of the carbonaceous deposits. In the case of NiCe M, it was completely reactivated after the regeneration step, as the curve of ethanol conversion of the regenerated sample practically overlapped with that of the fresh one. However, considering hydrogen yield, an even faster deactivation is visible, with no hydrogen production after just 2 h. This apparent discrepancy, of the same conversion but different yield, is due to a different selectivity, indicating that some changes in the nature of the material occurred.

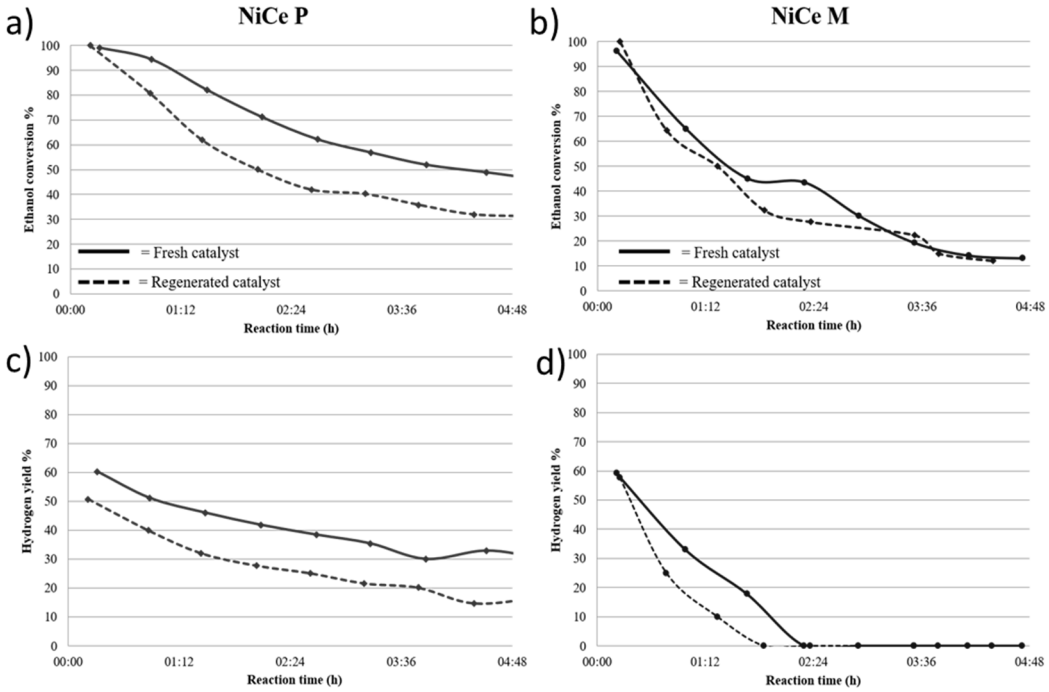

Figure 9. Ethanol steam reforming on fresh (solid lines) and reactivated (dotted lines) catalysts. Ethanol conversion (**a**) NiCe P and (**b**) NiCe M and hydrogen yield (**c**) NiCe P and (**d**) NiCe M vs. reaction time.

As a matter of fact, the causes of catalysts deactivation were quite different for two samples. In fact, the catalyst prepared via microemulsions, despite the faster deactivation with time, seemed to be reactivated during the regeneration step. Therefore, its complete deactivation in the first run was probably due to a reversible coke deposition. SEM analyses performed on used NiCe M catalyst had shown that it was almost completely covered by a compact form of carbon, either polymeric or graphitic. Such coke can be oxidized during regeneration step. On the contrary, the catalyst prepared via precipitation is more stable over time, but it cannot be fully regenerated in air. For this used sample, SEM pictures have shown that only a small portion of metal was covered by coke deposits, and it could be easily removed during the oxidative treatment of regeneration. Hence, this is not the main cause of deactivation, and sintering of the active phase had probably occurred. As demonstrated by TPR technique, NiCe P presented a lower interaction between support and active phase, and this could have determined its easier sintering.

4. Conclusions

The effect of the preparation method, namely, precipitation and microemulsion synthesis, has been evaluated for nickel–ceria-based catalysts. As expected, the microemulsion approach allowed us to prepare materials with smaller NiO dimensions and a defined interaction between NiO and support stronger than in the catalysts with precipitated supports, as evidenced by TPR analyses. At the same time, the samples prepared via precipitation had higher surface areas, well-defined spherical particles, and higher crystallinity. Therefore, the preparation method strongly affected the structural and chemical properties of catalysts. In ethanol steam reforming, the catalysts prepared via precipitation showed higher catalytic activity and stability, while those prepared via microemulsion deactivated very fast. Similar trends were found for La-promoted supports. Nevertheless, after the oxidative regeneration treatment, the NiCe P catalyst did not fully regain its properties, while NiCe M was completely reactivated. This indicated that the reasons for catalyst deactivation should be quite different. For catalysts prepared by precipitation, the

deactivation was mostly due to sintering of the nickel particles that were not strongly interacting with the support. On the contrary, strong interaction between active phase and support in NiCe M preserved the material from sintering. However, the lower surface area and the low degree of crystallinity led to a rapid deactivation of the material caused by coke deposition.

Author Contributions: Conceptualization, M.S. and V.C.; methodology, A.M.A.; formal analysis, C.P.; investigation, E.G.; data curation, F.M.; writing original draft preparation, review and editing, F.M.; supervision, M.S.; funding acquisition M.S. and V.C.C. All authors have read and agreed to the published version of the manuscript.

Funding: This research was funded by MINECO project CTQ2015-71823-R and MICINN project RTI2018-101604-B-I00 (Spain).

Acknowledgments: The technical help of M. Sanchez with SEM measurements is gratefully acknowledged.

Conflicts of Interest: The authors declare no conflict of interest.

References

1. IEA. The Future of Hydrogen, IEA, Paris. Available online: https://www.iea.org/reports/the-future-of-hydrogen (accessed on 12 November 2020)
2. Wang, J.; Chen, H.; Tian, Y.; Yao, M.; Li, Y. Thermodynamic analysis of hydrogen production for fuel cells from oxidative steam reforming of methanol. *Fuel* **2012**, *97*, 805–811, doi:10.1016/j.fuel.2012.03.008.
3. Ball, M.; Weeda, M. The hydrogen economy—Vision or reality? *Int. J. Hydrogen Energy* **2015**, *40*, 7903–7919, doi:10.1016/j.ijhydene.2015.04.032.
4. Navarro, R.M.; Peña, A.M.A.; Fierro, J.G. Hydrogen Production Reactions from Carbon Feedstocks: Fossil Fuels and Biomass. *Chem. Rev.* **2007**, *107*, 3952–3991, doi:10.1021/cr0501994.
5. Abe, J.; Popoola, A.; Ajenifuja, E.; Popoola, O. Hydrogen energy, economy and storage: Review and recommendation. *Int. J. Hydrogen Energy* **2019**, *44*, 15072–15086, doi:10.1016/j.ijhydene.2019.04.068.
6. Gallucci, F.F.; Basile, A.A.; Tosti, S.; Iulianelli, A.; Drioli, E. Methanol and ethanol steam reforming in membrane reactors: An experimental study. *Int. J. Hydrogen Energy* **2007**, *32*, 1201–1210, doi:10.1016/j.ijhydene.2006.11.019.
7. Liu, Z.; Senanayake, S.D.; Rodriguez, J.A. Catalysts for the Steam Reforming of Ethanol and Other Alcohols. *Ethanol* **2019**, *574*, 133–158, doi:10.1016/b978-0-12-811458-2.00005-5.
8. Martinelli, M.; Watson, C.D.; Jacobs, G. Sodium doping of Pt/m-ZrO2 promotes C–C scission and decarboxylation during ethanol steam reforming. *Int. J. Hydrogen Energy* **2020**, *45*, 18490–18501, doi:10.1016/j.ijhydene.2019.08.111.
9. Mironova, E.; Lytkina, A.; Ermilova, M.; Efimov, M.N.; Zemtsov, L.; Orekhova, N.; Karpacheva, G.; Bondarenko, G.; Muraviev, D.; Yaroslavtsev, A.B. Ethanol and methanol steam reforming on transition metal catalysts supported on detonation synthesis nanodiamonds for hydrogen production. *Int. J. Hydrogen Energy* **2015**, *40*, 3557–3565, doi:10.1016/j.ijhydene.2014.11.082.
10. Mattos, L.V.; Jacobs, G.; Davis, B.H.; Noronha, F.B. Production of Hydrogen from Ethanol: Review of Reaction Mechanism and Catalyst Deactivation. *Chem. Rev.* **2012**, *112*, 4094–4123, doi:10.1021/cr2000114.
11. Słowik, G.; Greluk, M.; Rotko, M.; Machocki, A. Evolution of the structure of unpromoted and potassium-promoted ceria-supported nickel catalysts in the steam reforming of ethanol. *Appl. Catal. B: Environ.* **2018**, *221*, 490–509, doi:10.1016/j.apcatb.2017.09.052.
12. Xu, W.; Liu, Z.; Johnston-Peck, A.C.; Senanayake, S.D.; Zhou, G.; Stacchiola, D.; Stach, E.A.; Rodriguez, J.A. Steam Reforming of Ethanol on Ni/CeO2: Reaction Pathway and Interaction between Ni and the CeO2 Support. *ACS Catal.* **2013**, *3*, 975–984, doi:10.1021/cs4000969.
13. Rodrigues, T.S.; E Silva, F.A.; Candido, E.G.; Da Silva, A.G.M.; Geonmonond, R.D.S.; Camargo, P.H.C.; Linardi, M.; Fonseca, F. Ethanol steam reforming: understanding changes in the activity and stability of Rh/MxOy catalysts as function of the support. *J. Mater. Sci.* **2019**, *54*, 11400–11416, doi:10.1007/s10853-019-03660-z.
14. Arslan, A.; Doğu, T. Effect of calcination/reduction temperature of Ni impregnated CeO2–ZrO2 catalysts on hydrogen yield and coke minimization in low temperature reforming of ethanol. *Int. J. Hydrogen Energy* **2016**, *41*, 16752–16761, doi:10.1016/j.ijhydene.2016.07.082.
15. Montero, C.; Remiro, A.; Benito, P.L.; Bilbao, J.; Gayubo, A.G. Optimum operating conditions in ethanol steam reforming over a Ni/La2O3-αAl2O3 catalyst in a fluidized bed reactor. *Fuel Process. Technol.* **2018**, *169*, 207–216, doi:10.1016/j.fuproc.2017.10.003.
16. Di Michele, A.; Dell'Angelo, A.; Tripodi, A.; Bahadori, E.; Sànchez, F.; Motta, D.; Dimitratos, N.; Rossetti, I.; Ramis, G.; Sanchez, F. Steam reforming of ethanol over Ni/MgAl2O4 catalysts. *Int. J. Hydrogen Energy* **2019**, *44*, 952–964, doi:10.1016/j.ijhydene.2018.11.048.

17. Compagnoni, M., Tripodi, A., Di Michele, A., Sassi, A.P., Signoretto, M., Rossetti, I. Low temperature ethanol steam reforming for process intensification: New Ni/MOx–ZrO2 active and stable catalysts prepared by flame spray pyrolysis. *Int. J. Hydrogen Energy* **2017**, *42*, 28193–28213, doi:10.1016/j.ijhdene.2017.09.123.
18. Wu, Z.; Li, M.; Overbury, S.H. On the structure dependence of CO oxidation over CeO2 nanocrystals with well-defined surface planes. *J. Catal.* **2012**, *285*, 61–73, doi:10.1016/j.jcat.2011.09.011.
19. Manzoli, M.; Avgouropoulos, G.; Tabakova, T.; Papavasiliou, J.; Ioannides, T.; Boccuzzi, M.M.A.F. Preferential CO oxidation in H2-rich gas mixtures over Au/doped ceria catalysts. *Catal. Today* **2008**, *138*, 239–243, doi:10.1016/j.cattod.2008.05.001.
20. Pizzolitto, C.; Menegazzo, F.; Ghedini, E.; Innocenti, G.; Di Michele, A.; Cruciani, G.; Cavani, F.; Signoretto, M. Increase of Ceria Redox Ability by Lanthanum Addition on Ni Based Catalysts for Hydrogen Production. *ACS Sustain. Chem. Eng.* **2018**, *6*, 13867–13876, doi:10.1021/acssuschemeng.8b02103.
21. Aneggi, E.; Boaro, M.; Colussi, S.; de Leitenburg, C.; Trovarelli, A. Ceria-Based Materials in Catalysis: Historical Perspective and Future Trends. In *Handbook on the Physics and Chemistry of Rare Earths*; Elsevier: Amsterdam, The Netherlands, 2016; doi:10.1016/bs.hpcre.2016.05.002.
22. Menegazzo, F.; Pizzolitto, C.; Ghedini, E.; Di Michele, A.; Cruciani, G.; Signoretto, M. Development of La Doped Ni/CeO2 for CH4/CO2 Reforming. *C* **2018**, *4*, 60, doi:10.3390/c4040060.
23. Laguna, Óscar H.; Centeno, M. Ángel; Boutonnet, M.; Odriozola, J. Au-supported on Fe-doped ceria solids prepared in water-in-oil microemulsions: Catalysts for CO oxidation. *Catal. Today* **2016**, *278*, 140–149, doi:10.1016/j.cattod.2016.05.059.
24. Elias, J.S.; Risch, M.; Giordano, L.; Mansour, A.N.; Shao-Horn, Y. Structure, Bonding, and Catalytic Activity of Monodisperse, Transition-Metal-Substituted CeO2Nanoparticles. *J. Am. Chem. Soc.* **2014**, *136*, 17193–17200, doi:10.1021/ja509214d.
25. Ferencz, Z.; Erdőhelyi, A.; Baán, K.; Oszkó, A.; Óvári, L.; Kónya, Z.; Papp, C.; Steinrück, H.-P.; Kiss, J. Effects of Support and Rh Additive on Co-Based Catalysts in the Ethanol Steam Reforming Reaction. *ACS Catal.* **2014**, *4*, 1205–1218, doi:10.1021/cs500045z.
26. Eriksson, S.; Nylén, U.; Rojas, S.; Boutonnet, M. Preparation of catalysts from microemulsions and their applications in heterogeneous catalysis. *Appl. Catal. A: Gen.* **2004**, *265*, 207–219, doi:10.1016/j.apcata.2004.01.014.
27. Brunauer, S.; Emmett, P.H.; Teller, E. Adsorption of Gases in Multimolecular Layers. *J. Am. Chem. Soc.* **2005**, *60*, 309–319, doi:10.1021/ja01269a023.
28. Barrett, E.P.; Joyner, L.G.; Halenda, P.P. The Determination of Pore Volume and Area Distributions in Porous Substances. I. Computations from Nitrogen Isotherms. *J. Am. Chem. Soc.* **1951**, *73*, 373–380, doi:10.1021/ja01145a126.
29. Rossetti, I.; Lasso, J.; Nichele, V.; Signoretto, M.; Finocchio, E.; Ramis, G.; Di Michele, A. Silica and zirconia supported catalysts for the low-temperature ethanol steam reforming. *Appl. Catal. B: Environ.* **2014**, *150–151*, 257–267, doi:10.1016/j.apcatb.2013.12.012.
30. Pinna, F. Supported metal catalysts preparation. *Catal. Today* **1998**, *41*, 129–137, doi:10.1016/s0920-5861(98)00043-1.
31. Balbuena, P.B.; Gubbins, K.E. Theoretical interpretation of adsorption behavior of simple fluids in slit pores. *Langmuir* **1993**, *9*, 1801–1814, doi:10.1021/la00031a031.
32. Thommes, M.; Kaneko, K.; Neimark, A.V.; Olivier, J.P.; Rodriguez-Reinoso, F.; Rouquerol, J.; Sing, K.S. Physisorption of gases, with special reference to the evaluation of surface area and pore size distribution (IUPAC Technical Report). *Pure Appl. Chem.* **2015**, *87*, 1051–1069, doi:10.1515/pac-2014-1117.
33. Manzoli, M.; Menegazzo, F.; Signoretto, M.; Cruciani, G.; Pinna, F. Effects of synthetic parameters on the catalytic performance of Au/CeO2 for furfural oxidative esterification. *J. Catal.* **2015**, *330*, 465–473, doi:10.1016/j.jcat.2015.07.030.
34. Nichele, V.; Signoretto, M.; Menegazzo, F.; Rossetti, I.; Cruciani, G. Hydrogen production by ethanol steam reforming: Effect of the synthesis parameters on the activity of Ni/TiO2 catalysts. *Int. J. Hydrogen Energy* **2014**, *39*, 4252–4258, doi:10.1016/j.ijhydene.2013.12.178.
35. Menegazzo, F.; Burti, P.; Signoretto, M.; Manzoli, M.; Vankova, S.; Boccuzzi, F.; Pinna, F.; Strukul, G. Effect of the addition of Au in zirconia and ceria supported Pd catalysts for the direct synthesis of hydrogen peroxide. *J. Catal.* **2008**, *257*, 369–381, doi:10.1016/j.jcat.2008.05.019.
36. Pinton, N.; Vidal, M.; Signoretto, M.; Martínez-Arias, A.; A., V.C.C. Ethanol steam reforming on nanostructured catalysts of Ni, Co and CeO 2: Influence of synthesis method on activity, deactivation and regenerability. *Catal. Today* **2017**, *296*, 135–143, doi:10.1016/j.cattod.2017.06.022.